Submitted to Visualization in Biomedical Computing (VBC) '96

A Robust Point Matching Algorithm for Autoradiograph Alignment

Anand Rangarajan[1], Eric Mjolsness[2], Suguna Pappu[1,3], Lila Davachi[4], Patricia S. Goldman-Rakic[4] and James S. Duncan[1,5]

Department of [1]Diagnostic Radiology, [3]Neuroengineering and Neuroscience Center (NNC),
[4]Section of Neurobiology and [5]Department of Electrical Engineering
Yale University

[2]Department of Computer Science and Engineering
University of California San Diego (UCSD)

Abstract

Neuroimaging of the human brain has opened the way for a genuine understanding of human cognition; but the circuitry and cellular basis of the extraordinary information processing capacity of humans can be addressed only in experimental animals such as nonhuman primates. Current research in nonhuman primates at Yale is concerned with elucidating functional maps of cortical activity using the 2-DG autoradiographic method developed by (Sokoloff et al., 1977). This method requires sacrifice of the animal and sectioning of the brain into serial sections followed by production of autoradiographs of individual brain sections which are not in register.

We have developed a new automated alignment method to reconstitute the autoradiographs. All previous alignment methods are unable to automatically correct for cuts, tears and natural differences between slices. In contrast, our newly developed alignment methods automatically find the spatial mapping and robustly account for the natural and artifactual differences between slices by applying the powerful mechanism of outlier rejection adapted from the robust statistics literature. Our approach results in an automated algorithm that extracts edges from the slices, finds the 2-D spatial mapping and the homologies between slices and robustly discards the extraneous and/or missing edges via the mechanism of outlier rejection.

1 Introduction

Functional studies of cortical circuitry can be performed by observing radiotracer uptake in autoradiographs. Here, local cerebral glucose utilization (LCGU) can be observed in order to study how the brain performs certain cognitive tasks. Current research in nonhuman primates in the Section of Neurobiology, Yale University School of Medicine (Friedman and Goldman-Rakic, 1994) is concerned with elucidating functional maps of cortical activity using the 2-DG autoradiographic method developed by (Sokoloff et al., 1977; Kennedy et al., 1978). This method requires sacrifice of the animal and sectioning of the brain into serial sections followed by production of autoradiographs of extremely fine ($\simeq 10\mu$) slices and observing and quantitatively analyzing radiotracer uptake in each slice. Because of the extremely high spatial resolution of this technique, it is the case that these studies are the likely gold standard to which a number of imaging studies that attempt to measure cognitive function *in vivo* will be compared (e.g. fMRI, PET, SPECT).

One current downside of analyzing these autoradiographs, however, are the very large amounts of data that are produced. Each one of four sections of a monkey brain that are typically analyzed may be used to generate 1000 individual brain slices which are themselves not in register. While the spatial resolution of the individual 2-D slices is very high, the 3-D spatial structure available for example in volumetric MRI is lost. Due to the unavailability of 3-D MRI of the same primate and due to the lack of automated autoradiograph–MRI registration methods, the rich and internally coherent anatomical structure of 3-D MRI remains unutilized in current 3-D primate autoradiograph reconstruction [or "reconstitution" (Kim et al., 1995)]. To date, these difficulties have limited researchers to analyzing only small portions of the brain at a time and thus has not permitted analysis of relationships between spatially disparate (yet possibly cognitively-related) regions. There is a current need for the development of systems that robustly and efficiently portray the globally distributed processing known to exist in the primate brain.

Since we have access to functional (metabolic) 2-DG autoradiographs and 3-D MRI of the same primate, we would like to reconstitute the 3-D autoradiograph volume using the 3-D MRI as an anatomical roadmap. Thereby we overcome the "leaning tower of Pisa" problem inherent in autoradiograph reconstitution in the absence of internally coherent 3-D anatomical information. Reconstitution is broadly divided into two stages: i) Align the autoradiograph slices and ii) Register the slices with MRI.

In this paper, we present a solution to the first problem by designing a new automated autoradiograph alignment method. The method is based on a newly developed *robust point matching* (RPM) algorithm (Gold et al., 1995; Rangarajan et al., 1996) that simultaneously finds homologies (correspondence) and similarity transformation parameters (rotation, translation and scale) between sequential pairwise slices. The inability of previous automated alignment methods to correct for artifacts like cuts and tears in the slices and for systematic variation from slice to slice is hereby accounted for. Our method is robust to this variability in the statistical sense of rejecting artifacts and natural differences as *outliers*—point features in either slice that have no homologies in the other slice (Black and Rangarajan, 1995).

A similarity transformation is sufficient since in stage 2, we plan to register the autoradiographs with 3-D MRI using affine and/or other warping transformations. Other alignment methods which introduce shearing transformations to align the slices face the problem of validation. Without 3-D

MRI, there is no "ground-truth" 3-D information available to validate shears and other warps of the autoradiograph slices. Since we have 3-D MRI available, our alignment method finds a similarity transformation to approximately register the slices.

In Section 3, we present a method to align individual autoradiograph slices. First, edge detection is performed on the slices. Point features (with only location information) are obtained from the edge images. The RPM algorithm is then executed on the point sets to obtain a similarity transformation (rotation, translation, scale). We refrain from introducing shear and other warping deformations into the catalog of allowed spatial transformations until the next stage of registration with MRI. While the registration and warping of the autoradiograph volume onto MRI is beyond the scope of this paper, it plays an important role in ongoing work on autoradiograph reconstitution.

2 Previous Work

Automated Autoradiograph alignment is the primary goal of this study and we will present a novel alignment method in Section 3. If previous automated methods achieve autoradiograph alignment, why do we require another method? The *principal flaw* that other methods share in comparison to our RPM method is that they are not *robust* (Black and Rangarajan, 1995) in the statistical sense of automatically rejecting cuts, tears and natural variations between slices as *outliers*—point features in either set that have no homologies in the other.

The principal autoradiograph alignment methods are i) principal axis/center of mass (Hibbard and Hawkins, 1988), ii) frequency domain cross correlation (Toga and Banerjee, 1993), iii) spatial domain cross correlation (Toga and Banerjee, 1993) and iv) the disparity analysis (Zhao et al., 1993) methods. (Most of these methods also perform autoradiograph–blockface video alignment. Since our data set does not have blockface video information, we are not including it as a specific aim of this study.) The principal axis method detects the center of mass of the two images, translates one image so that the center of masses coincide, then finds the principal axes using the eigenvector transform and aligns them via a rotation. The method is not robust to tears in the slices and also does not perform well when the images do not have bilateral symmetry. Cross correlation methods (either frequency or spatial domain) maximize the cross correlation with respect to the transformation parameters. This approach assumes densitometic consistency between slices. Consequently, the method is not robust to changes in the intensity patterns and when cuts and tears are present in the slices. A good comparison of these methods can be found in (Toga and Banerjee, 1993). The disparity analysis method is based on optical flow. An affine transformation is used to regularize the flow field at each point. The method works with either boundary or intensity information. Consequently, the method is dependent either on good boundary detection or on densitometric consistency and is not robust.

General purpose feature matching methods exist in the literature (Jiang et al., 1992; Mangin et al., 1992; Besl and McKay, 1992; Lavallee, 1996). All these methods are based on minimizing the distances between points in one set and the closest point in the other set with respect to the spatial transformation. Consequently, the distance measures are brittle, sensitive to changes in feature location and to false positives in the detection of closest points. Since good feature extraction is assumed by these methods, they are unable to robustly correct for missing and/or spurious information.

3 Automated Autoradiograph Alignment Approach

In Figure 1, two primate autoradiograph slices (slice 379 and slice 380) are shown.

Autoradiography: A rhesus monkey was habituated over many months to perform working memory (WM) tasks under restrained conditions. An arterial catheter was introduced into one of the femoral arteries and ^{14}C-deoxy-D-glucose (2DG) of approximately 100μCi/kg was injected through the cannula of the awake rhesus monkey which was kept restrained in a primate chair. Immediately after the injection, the animal performed the task uninterruptedly for an entire 45 minute period. After 45 minutes, the primate was sacrificed, perfused and the brain was frozen at -70°C. 20μm thick frozen sections were cut in a cryostat. The sections along with isotope standards had a seven day exposure after which the film was developed. Autoradiographs of brain sections, togther with each film's set of ^{14}C standards were digitized with a MCID computerized video image processing system. The computer used these standards to quantify radioactivity in each brain image by translating pixel-gray values to ^{14}C levels: these levels were then converted to LCGU rates. [For more details on autoradiograph acquisition, see (Friedman and Goldman-Rakic, 1994) and the excellent article in (McEachron et al., 1986) for background information.] While blockface video was not recorded for this dataset, 124 coronal T1-weighted MRI slices were obtained. With the availability of autoradiographs *and* 3-D MRI, our final goal is the simultaneous reconstitution and registration of the autoradiographs with MR.

We now describe the methodology for the alignment of the 2-D autoradiograph slices. A characteristic feature of the autoradiograph slices that are adjacent (for example slice 379 and 380 shown above) is overall similarity except for local areas of dissimilarity. Cuts, tears, irregular slicing and natural variations create local deformations from slice to slice. Since the slices are handled individually, there is a fairly significant change in orientation between adjacent slices. For all these reasons and others mentioned in Section 2, there is a need for a robust image matching method that finds similarity transformations (rotation, translation, scale) between slices and is stable to local deformations. Such an algorithm is the RPM method and as we shall demonstrate, there is great synergy in applying this method to our problem. Previous work (Gold et al., 1995; Rangarajan et al., 1996) with the RPM algorithm was confined to data generated synthetically or at best handwritten characters. There is no prior work detailing use of an edge detector to get point features followed by the RPM method. Specific application to autoradiograph alignment is even more novel.

Assume that the edge detection phase is completed and we have edge images corresponding to the autoradiograph slices. [As we shall describe later, a Canny edge detector (Canny, 1986) is sufficient to obtain edges with good localization.] High confidence edges alone are chosen after thresholding the edge images. The locations corresponding to the edges are then obtained from the edge images. Denote the edge location information from slice 1 and slice 2, $X_i,\ i = 1, 2, ..., N_1$ and $Y_j,\ j = 1, 2, ..., N_2$ respectively. N_1 and N_2 are the number of edge locations in the sets X and Y respectively. The RPM algorithm minimizes the following objective function (optimization problem):

$$\min_{M,\theta,t,s} E(M, R(\theta), t, s) = \sum_{i=1}^{N_1}\sum_{j=1}^{N_2} M_{ij} \|X_i - t - sR(\theta)Y_j\|^2 - \alpha \sum_{i=1}^{N_1}\sum_{j=1}^{N_2} M_{ij} \tag{1}$$

$$\text{subject to} \sum_{i=1}^{N_1} M_{ij} \leq 1,\ \sum_{j=1}^{N_2} M_{ij} \leq 1,\ \text{and } M_{ij} > 0. \tag{2}$$

Equation (1) describes an optimization problem from which the transformation parameters—rotation matrix $R(\theta)$, translation t, and scale s—can be obtained by minimization. However, (1) also sets up an optimization problem on the point correspondences. The variable M_{ij} is a correspondence variable which indicates when homologies have been found. If M_{ij} is one, feature "i" in slice 1 and feature "j" in slice 2 are homologies. The constraints on M_{ij} enforce one-to-one correspondence between homologies and also robustness (Black and Rangarajan, 1995): as shown in Figure 2 a point feature in one image may have no corresponding homology and should be discarded as a statistical outlier. The degree of robustness is enforced by the parameter α. If α is large, fewer points are discarded and vice-versa.

Automatically finding homologies is important because of the time consuming and labor intensive nature of manual selection. Automatically discarding features that have no homologies is important—otherwise the method would suffer from the same problems that beset intensity correlation.

We use a continuation method (Rangarajan and Chellappa, 1993) to perform the optimization of (1). The continuation method incorporates a temperature parameter β similar to simulated annealing methods of optimization but in contrast is completely deterministic and more efficient. Poor local minima are avoided by the continuation method. Our presentation will be quite terse. More details can be found in (Rangarajan et al., 1996; Gold et al., 1995).

Algorithm Summary:

Initialize β to β_{min}.

Solve for the correspondence variables M.

Solve in closed form for the similarity transformation (rotation, translation and scale parameters.

Iterate until convergence or until an iteration cap is exceeded.

Increase β and iterate until convergence or until $\beta > \beta_{max}$.

The method solves for the correspondence and the transformation parameters in turn. Given the correspondence (match) matrix M, closed-form solutions are found for the spatial transformation parameters; rotation angle θ, translation vector $[t_x, t_y]$ and scale s. We perform coordinate-descent w.r.t. each spatial transformation parameter until a suitable convergence criterion is achieved. While it is possible to simultaneously solve for the rotation and translation parameters as in (Walker et al., 1991), we have not done so here.

Given the transformation parameters $(R(\theta), t, s)$, we can solve for the match matrix: M_{ij} is first set to

$$M_{ij} = \exp\left[-\beta\left(\|X_i - t - sR(\theta)Y_j\|^2 - \alpha\right)\right] \tag{3}$$

followed by an *iterated row and column normalization* method to satisfy the row and column constraints in (2):

$$M_{ij} \leftarrow \frac{M_{ij}}{\sum_{a=1}^{N_1} M_{aj}}, \; M_{ij} \leftarrow \frac{M_{ij}}{\sum_{b=1}^{N_1} M_{ib}} \tag{4}$$

The exponentiation is necessary to obtain non-negative values for the match matrix M. Subsequently, the row and column normalization method performs constraint satisfaction using this non-negative matrix. For more details on the exponentiation used in (3) and on the row and column normalization method of constraint satisfaction, please see (Rangarajan et al., 1996; Gold et al., 1995; Kosowsky and Yuille, 1994).

As the continuation parameter β is increased, the match matrix entries "harden"—they approach binary values. Outlier rejection occurs in the limit when $\beta \to \infty$ with the outliers becoming binary valued.

4 Results

Having described the method in general, we now apply it on the two autoradiograph slices (slice 379 and slice 380) shown in Figure 1.

Table 1: Registration parameters with and without knowledge of homologies.

	Rotation (in degrees)	Translation (in pixels)
Homologies unknown (RPM method)	5.1	[21,-5]
Homologies known	4.9	[23,0]

First we run a Canny edge detector (Canny, 1986) on each slice. The edge detector is a single scale (Gaussian filter with width σ) edge detector incorporating hysteresis and non-maximum suppression. Low t_l and high t_h threshold parameters can be specified for edge tracking. The parameters used for both slices were the program defaults—$\sigma = 1$, $t_l = 0$ and $t_h = 255$. The edge images shown in Figure 3 are $\simeq$ 475x350 each which is the same size as the original slices. Some gradations in edge strength are discernible from the edge images.

We now threshold the edge images to obtain binary images: the same threshold of 240 was chosen for both slices. The point sets X and Y are obtained from the binary images. The point sets are shown in Figure 4. Every fourth edge was chosen in constituting a point set. There were roughly 800 points in each point set.

Having obtained the point sets, we now execute the RPM algorithm. Exactly as described above, we specify an initial value for the continuation parameter $\beta_{initial} = 0.3$. The robustness parameter α was set to 5. A linear schedule was prescribed for β; $\beta^{(n+1)} = \beta^{(n)}/0.9$. When β reaches $\beta_{max} = 5$, the algorithm terminates. The maximum number of row and column normalizations in the correspondence step was 30. At each setting of β, we executed the inner loop of the algorithm a maximum of 3 times. Initial conditions are not very relevant. Since $\beta_{min} = 0.3$ is quite low, the algorithm sets the translation parameters to the difference between the centroids of the point sets. The final solution and overlay of the points sets is shown in Figure 5.

The x's and o's are from slice 379 and slice 380 respectively and indicate the coordinate locations of the edge (point) features. Note that a subset of the x's and o's do not match. The method has discarded them as outliers. The matrix M_{ij} has all zero rows (columns) corresponding to the outliers. all zero. The recovered registration parameters are shown in Table 1.

The top left corner of the X point set was the center of rotation. The scale factors in both cases were close to unity. The recovered registration parameters with and without assuming knowledge of corresponding homologies are very close to each other.

We have shown an initial study where autoradiograph slices are aligned using a novel edge feature matching method. The method jointly solves for the transformation parameters, rotation, translation and scale as well as the correspondences or homologies. The method also discards features that have no homologies. That the method is robust is demonstrated by the fact that we did not even have to edit the slice index label on the autoradiographs! The label number (380 for example) can be partially seen in Figure 1 and in the edge images as well. The method discarded the label number by employing outlier rejection (Black and Rangarajan, 1995).

We also executed the RPM algorithm on point sets derived from coronal slices 384 and 385 as well as slices 405 and 409. Slices 384 and 385 are displayed in Figure 6. After digitization, the slices were sampled into roughly a 475x350 pixels with an approximate pixel size of 100μm. As before Canny edges were obtained with no change in the filter width and the thresholds (low and high). The edge images are displayed in Figure 7. Point sets were extracted from the edge images (shown in Figure 8). There were roughly 3000 points in each point set. In contrast to the previous experiment where every fourth point was taken to yield approximately 800 points, this time every tenth point was chosen from each set for the RPM algorithm. The results are shown in Figure 9. The recovered registration parameters were $\theta = 8.9°$ and $t = [-18, 10]$. The scale factor was again very close to unity. Another difference from the previous experiment is the center of rotation. This time the center of slice 384 was the center of rotation. Since the slices don't match up as well as slices 379 and 380, local differences on the boundary contours can be seen. This experiment serves to demonstrate that the RPM algorithm can also be used with a small subset of the points. A more efficient strategy might be a coarse-to-fine approach (Lu and Mjolsness, 1994) with the Canny filter scales chosen to get large scale edges first and then small scale edges.

The final experiment with slices 405 and 409 showcases the robustness property. Examine the slices shown in Figure 10. While there is a much larger rotation difference between the slices, the major difference is the top fifth of slice 409 which is missing in slice 405. The edge images and point sets are shown in Figures 11 and 12 respectively. There was no change from the parameters used in the previous experiments. (Slice 405 is 260x160 pixels and the point set has 1000 points. Slice 409 is 275x220 with the point set containing 1500 points.) Every third point was chosen for the RPM algorithm. The results are shown in Figure 13. Despite the large differences between the slices, the RPM algorithm had no difficulty in rejecting the extraneous information as outliers. The recovered transformation parameters were $\theta = 12.8°$ and $t = [-1, 4.6]$. The center of the "o" point set was the center of rotation. The scale parameter was unity.

5 Discussion

The 2-DG method developed in (Sokoloff et al., 1977) can be used to obtain high resolution functional (metabolic) maps of the primate brain in the form of autoradiographs. While autoradiograph slices are of very high resolution, the large numbers of slices acquired create data processing problems. A block of monkey brain can result in thousands of slices and the slices may have cuts and tears creating further problems for reconstitution. The tedium of data analysis in this area of research is a serious impediment to unique studies that hold promise for bridging human cognition with anatomical and physiological data obtainable from an animal model.

We have developed a new automated alignment method which is based on Canny edge detection followed by a robust point matching (RPM) algorithm that solves for a similarity transformation between slices. The method automatically finds homologies, and rejects non-homologies as outliers. The alignment method is the first stage in a two stage procedure that i) aligns sequential, pairwise autoradiograph slices and ii) registers and warps the autoradiograph volume onto 3-D MRI. While we have not discussed registration with MRI in this paper, it plays a crucial role in lending 3-D volumetric coherence to the process of autoradiograph reconstitution. Finally, the automated alignment method resulting from this study can be applied to other areas such as registration of MRI to anatomical atlases, and intermodality registration in general.

References

Besl, P. J. and McKay, N. D. (1992). A Method for Registration of 3-D Shapes. *IEEE Trans. Patt. Anal. Mach. Intell.*, 14(2):239–256.

Black, M. and Rangarajan, A. (1995). On the Unification of Line Processes, Outlier Detection and Robust Statistics with Applications in Early Vision. *Intl. J. Computer Vision*. (in press).

Canny, J. (1986). A Computational Approach to Edge Detection. *IEEE Trans. on Pattern Analysis and Machine Intelligence*, 8(6):679–698.

Friedman, H. R. and Goldman-Rakic, P. S. (1994). Coactivation of Prefrontal Cortex and Inferior Parietal Cortex in Working Memory Tasks Revealed by 2DG Functional Mapping in the Rhesus Monkey. *J. Neuroscience*, 14(5):2775–2788.

Gold, S., Lu, C. P., Rangarajan, A., Pappu, S., and Mjolsness, E. (1995). New Algorithms for 2-D and 3-D Point Matching: Pose Estimation and Correspondence. In Tesauro, G., Touretzky, D., and Alspector, J., editors, *Advances in Neural Information Processing Systems 7*, pages 957–964. MIT Press, Cambridge, MA.

Hibbard, L. S. and Hawkins, R. A. (1988). Objective Image Alignment for Three–Dimensional Reconstruction of Digital Autoradiograms. *J. Neurosci. Methods*, 26:55–75.

Jiang, H., Holton, K., and Robb, R. (1992). Image Registration of Multi–Modality 3-D Medical Images by Chamfer Matching. In *Proc. SPIE Biomedical Image Processing and Three–Dimensional Microscopy*, volume 1660, pages 356–366, Bellingham, WA. SPIE Press.

Kennedy, C., Sakurada, O., Shinohara, M., Jehle, J., and Sokoloff, L. (1978). Local Cerebral Glucose Utilization in the Normal Conscious Macaque Monkey. *Annals of Neurology*, 4:293–301.

Kim, B., Frey, K. A., Mukhopadhyay, S., Ross, B. D., and Meyer, C. R. (1995). Co-Registration of MRI and Autoradiography of Rat Brain in Three–Dimensions following Automatic Reconstruction of 2-D data set. In Ayache, N., editor, *Computer Vision, Virtual Reality and Robotics in Medicine*, volume 905 of *Lecture Notes in Computer Science*, pages 262–271. Springer–Verlag.

Kosowsky, J. J. and Yuille, A. L. (1994). The Invisible Hand Algorithm: Solving the Assignment Problem with Statistical Physics. *Neural Networks*, 7(3):477–490.

Lavallee, S. (1996). Registration for Computer Integrated Surgery: Methodology and state of the art. In Taylor, R., Lavallee, S., Burdea, G., and Mosges, R., editors, *Computer Integrated Surgery*, pages 77–97. MIT Press.

Lu, C. P. and Mjolsness, E. (1994). Two-Dimensional Object Localization by Coarse-to-Fine Correlation Matching. In Cowan, J., Tesauro, G., and Alspector, J., editors, *Advances in Neural Information Processing Systems 6*, pages 985–992. Morgan Kaufmann, San Francisco, CA.

Mangin, J.-F., Frouin, V., and Bendriem, B. (1992). Nonsupervised 3D registration of PET and MRI data using chamfer matching. In *Proc. of the Nucl. Sci. Symp./Med. Imag. Conf.*, volume 2, pages 1262–1267. IEEE Press.

McEachron, D. L., Adler, N. T., and Tretiak, O. J. (1986). Two Views of Functional Mapping and Autoradiography. In McEachron, D. L., editor, *Functional Mapping in Biology and Medicine: Computer Assisted Autoradiography*, volume 11 of *Experimental Biology and Medicine: Monographs on Interdisciplinary Topics*, pages 1–46. Karger, Basel.

Rangarajan, A. and Chellappa, R. (1993). A Continuation Method for Image Estimation using the Adiabatic Approximation. In Chellappa, R. and Jain, A. K., editors, *Markov Random Fields: Theory and Application*, chapter 4, pages 69–91. Acad. Press.

Rangarajan, A., Gold, S., and Mjolsness, E. (1996). A Novel Optimizing Network Architecture with Applications. *Neural Computation*, 8(5):???–??? (in press).

Sokoloff, L., Revich, M., Kennedy, C., DesRosiers, M. H., Patlak, C. S., Pettigrew, K. D., Sakurada, O., and Shinohara, M. (1977). The C14-deoxyglucose method for the measurement of local cerebral glucose utilization: theory, procedure, and normal values in the conscious and anesthetized albino rat. *J. Neurochem.*, 28:897–916.

Toga, A. W. and Banerjee, P. K. (1993). Registration revisited. *J. Neurosci. methods*, 48:1–13.

Walker, M. W., Shao, L., and Volz, R. (1991). Estimating 3-D location parameters using dual number quaternions. *CVGIP: Image Understanding*, 54(3):358–367.

Zhao, W., Young, T. Y., and Ginsberg, M. D. (1993). Registration and Three-Dimensional Reconstruction of Autoradiographic Images by the Disparity Analysis Method. *IEEE Transactions on Medical Imaging*, 12(4):782–791.

List of Figures

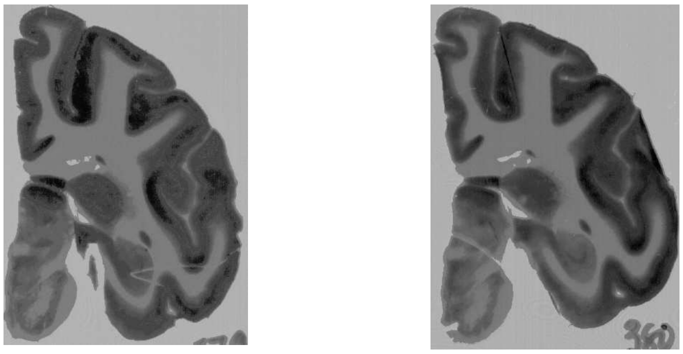

(a) (b)

Figure 1: (a) Slice 379 and (b) slice 380 of primate autoradiographs of functional (metabolic) activation. The coronal slices correspond to the left parietal and temporal cortex. After digitization, the slices were sampled down into $\simeq$ 475x350 pixels each with a resulting spatial resolution of $\simeq 100\mu$m.

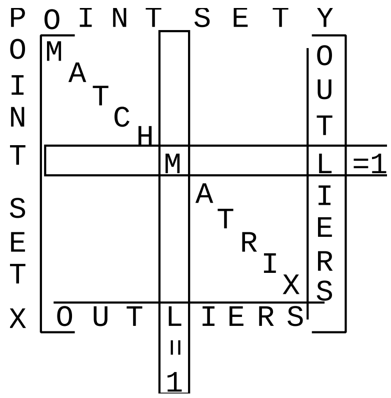

Figure 2: The Match Matrix. The points in the set X (the columns) are matched to the points in the set Y (the rows). When a point has no homology in the other set an entire column (row) has zero entries and the corresponding outliers turns "on".

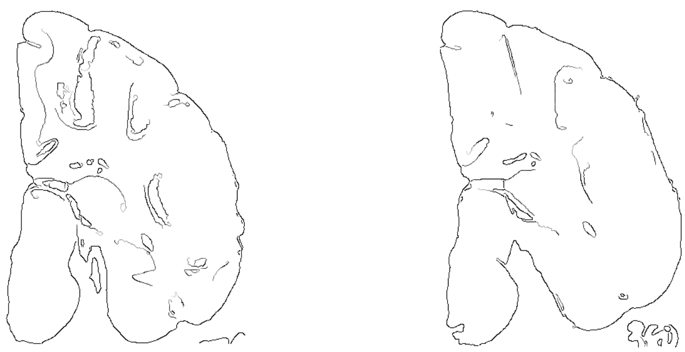

(a) (b)

Figure 3: Canny edge images corresponding to the autoradiograph slices of Figure 1. Note the number of edges in (a) that do not appear in (b). While we have not dwelled on the instability of edge detection, it is yet another reason for our strong emphasis on robustness.

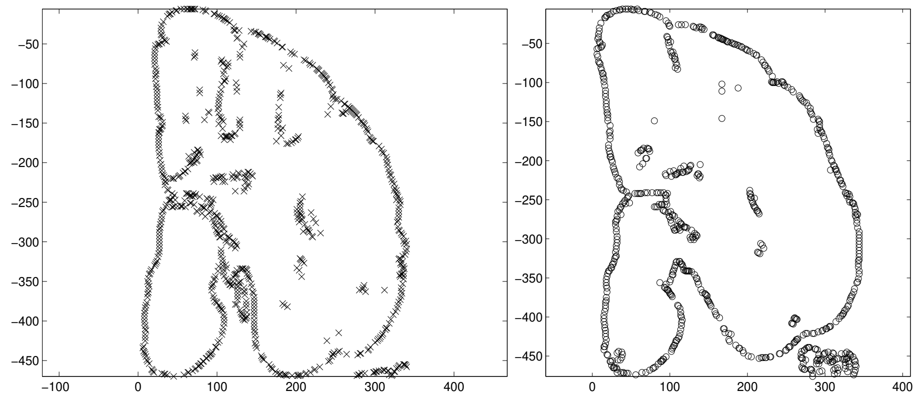

Figure 4: Point sets corresponding to the Canny edge images. Every fourth edge was taken yielding $\simeq$800 points per point set. Slice 379 and slice 380 are the X and Y point sets respectively.

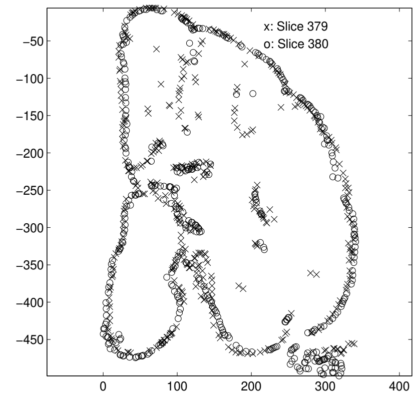

Figure 5: Final solution found by the method. Again note the number of (mostly internal) x′s and o′s that do not match but remain isolated during overlay. These have been rejected as outliers and play no role towards the final stages of the RPM algorithm.

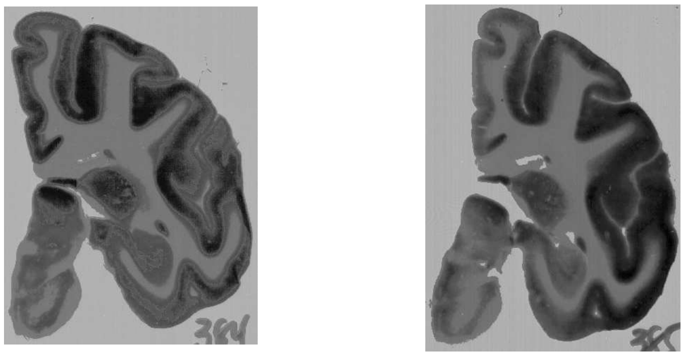

(a) (b)

Figure 6: (a) Slice 384 and (b) slice 385.

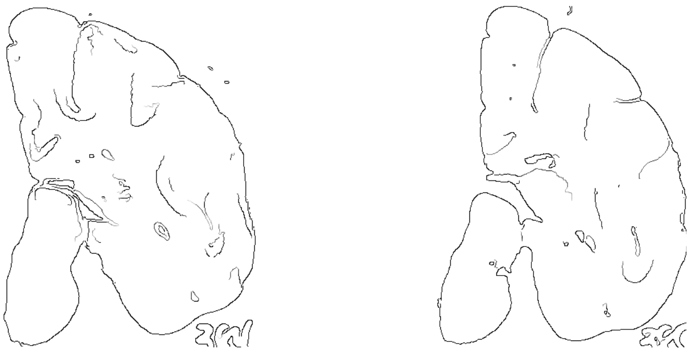

(a) (b)

Figure 7: Canny edge images corresponding to the autoradiograph slices 384 and 385.

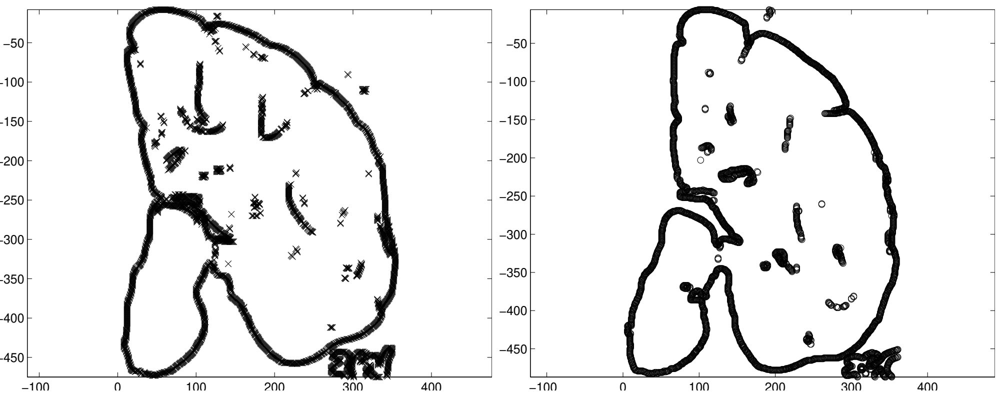

Figure 8: Point sets corresponding to the Canny edge images.

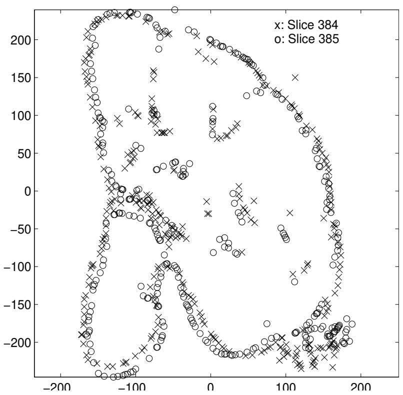

Figure 9: Final solution found by the method.

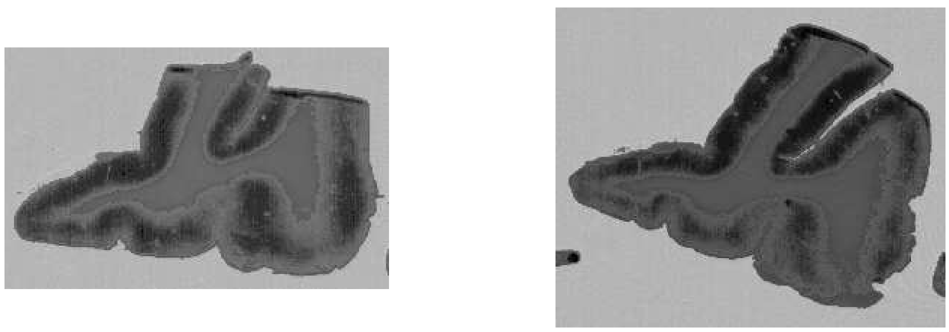

(a) (b)

Figure 10: (a) Slice 405 and (b) slice 409.

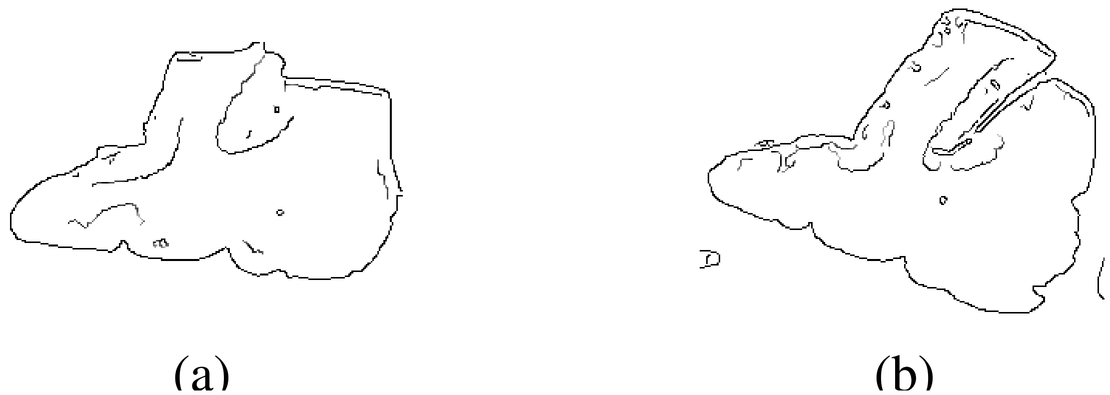

Figure 11: Canny edge images corresponding to the autoradiograph slices 405 and 409.

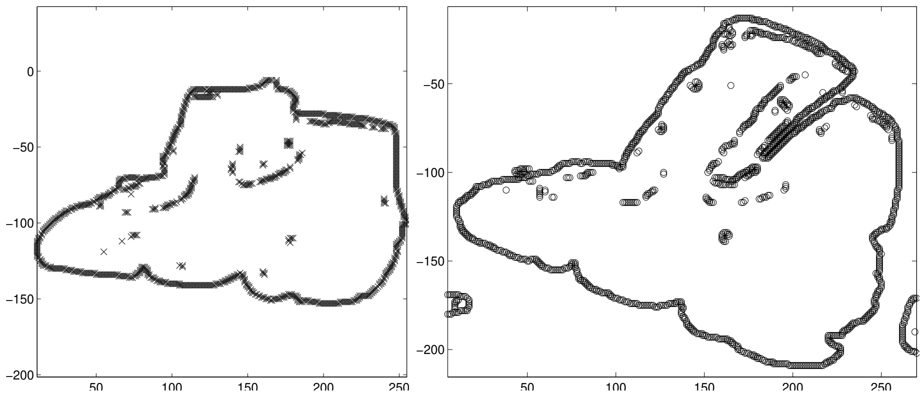

Figure 12: Point sets corresponding to the Canny edge images.

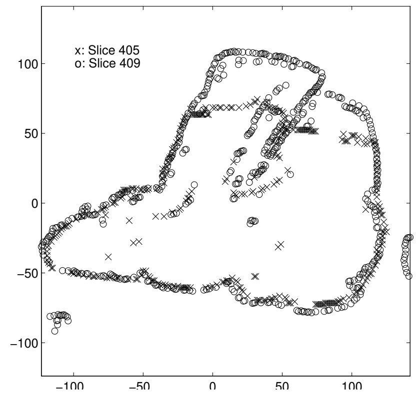

Figure 13: Final solution found by the method.